

RESEARCH

Open Access



First-in-human evaluation of memory-like NK cells with an IL-15 super-agonist and CTLA-4 blockade in advanced head and neck cancer

Roman M. Shapiro^{1†}, Michal Sheffer^{1†}, Matthew A. Booker², Michael Y. Tolstorukov², Grace C. Birch¹, Moshe Sade-Feldman^{3,4}, Jacy Fang^{3,4}, Shuqiang Li^{4,5}, Wesley Lu⁵, Michela Ansuinelli¹, Remy Dulery^{1,6}, Mubin Tarannum¹, Joanna Baginska⁷, Nishant Dwivedi⁸, Ashish Kothari⁸, Livius Penter¹, Yasmin Z. Abdulhamid¹, Isabel E. Kaplan¹, Dinh Khanhlinh¹, Ravindra Uppaluri⁹, Robert A. Redd¹⁰, Sarah Nikiforow¹, John Koreth¹, Jerome Ritz¹, Catherine J. Wu¹, Robert J. Soiffer¹, Glenn J. Hanna^{1,7*†} and Rizwan Romee^{1*†}

Abstract

Background Cytokine induced memory-like natural killer (CIML NK) cells combined with an IL-15 super-agonist (N-803) are a novel modality to treat relapsed/refractory head and neck cancer.

Methods We report data from a phase I trial of haploidentical CIML NK cells combined with N-803 with or without ipilimumab (IPI) in relapsed/refractory head and neck cancer patients after a median of 6 prior lines of therapy. The trial adhered to a 3 + 3 dose de-escalation design, with primary endpoint being safety. High-resolution immunophenotypic and transcriptional profiling characterized the NK cells and their interacting partners in vivo.

Results The primary safety endpoint was established, with dose-limiting toxicity in 1/10 patients. A transient disease control rate correlated with donor NK cell expansion, the latter occurring irrespective of IPI. The combination of CIML NK cells with N-803 and IPI was associated with increased early NK cell proliferation, contraction of Treg: Tcon, rapid recovery of recipient CD8⁺ T cells, and subsequent accelerated rejection of donor NK cells.

Conclusions CIML NK cells combined with N-803 and ipilimumab to treat head and neck cancer is safe, and associated with a more proliferative NK cell phenotype. However, the combination leads to reduced HLA mismatched NK cell persistence, resulting in an important limitation affecting NK cell combination therapies in clinical trials. These results inform evaluation of CIML NK therapy for advanced malignancies, with considerations for combination with IPI.

Trial Registration NCT04290546.

[†]Roman M. Shapiro and Michal Sheffer co-first authors.

[†]Glenn J. Hanna and Rizwan Romee co-senior authors.

*Correspondence:

Glenn J. Hanna
glenn_hanna@dfci.harvard.edu
Rizwan Romee
rizwan_rome@dfci.harvard.edu

Full list of author information is available at the end of the article



© The Author(s) 2025. **Open Access** This article is licensed under a Creative Commons Attribution-NonCommercial-NoDerivatives 4.0 International License, which permits any non-commercial use, sharing, distribution and reproduction in any medium or format, as long as you give appropriate credit to the original author(s) and the source, provide a link to the Creative Commons licence, and indicate if you modified the licensed material. You do not have permission under this licence to share adapted material derived from this article or parts of it. The images or other third party material in this article are included in the article's Creative Commons licence, unless indicated otherwise in a credit line to the material. If material is not included in the article's Creative Commons licence and your intended use is not permitted by statutory regulation or exceeds the permitted use, you will need to obtain permission directly from the copyright holder. To view a copy of this licence, visit <http://creativecommons.org/licenses/by-nc-nd/4.0/>.

Keywords Clinical trial, Head and neck cancer, NK cells, Interleukin-15, Ipilimumab

Background

Head and neck cancer represents the sixth most common malignancy worldwide, accounting for 3% of all annual new malignancy diagnoses and with an annual incidence that has been rising over the past decade [1]. Relapsed/refractory head and neck cancer patients have a poor prognosis [2] and represent a population in need of novel therapies. Building on the clinical benefit observed with PD-1-directed immunotherapy [3, 4], the adoptive transfer of natural killer (NK) cell-based therapy represents one such novel immunotherapeutic platform [5]. While studies have shown that the role of NK cells in the tumor microenvironment is complex, in some cases potentially detrimental by virtue of acting as a checkpoint on B7H6⁺ expressing activated T cells and CAR T cells [6], a high NK cell infiltrative signature has been associated with a favorable prognosis in head and neck cancer and supports their net potential benefit in this context [7, 8].

Cytokine-induced memory-like (CIML) NK cells have increased capacity for in vivo expansion and persistence and demonstrate enhanced cytokine production and cytotoxicity to tumor targets [9, 10, 11]. The clinical translation of CIML NK cell therapy in early phase trials has shown promising results in myeloid disease [12, 13, 14]. The application of CIML NK cells for the treatment of relapsed/refractory head and neck cancer represents a natural evolution of this immunotherapy platform to a setting where it may offer therapeutic benefits when other options are limited.

IL-15 is a gamma-chain family cytokine that plays a key role in the differentiation and activation of NK cells [15]. N-803 is an IL-15 superagonist (IL-15sa) that consists of an IL-15 mutein with enhanced activity, an IL-15R- α sushi domain mimicking physiologic trans-presentation, and an IgG1-Fc scaffold which substantially increases its half-life [16]. This agent is associated with enhanced NK cell expansion and function in vivo, and has shown efficacy in prior trials leading to its approval in non-muscle invasive bladder cancer recently [17, 18, 19, 20].

In the current study, we sought to determine the safety of haploidentical donor-derived CIML NK cells in combination with N-803 with and without CTLA-4 blockade in a phase I trial. While IL-15 signaling does not expand Tregs, the recovery of these immunomodulatory cells following lymphodepletion and CIML NK cell infusion may potentially inhibit the activity of adoptively transferred donor NK cells [21]. As Tregs are known to constitutively express high levels of CTLA-4 both in the peripheral blood and tumor microenvironment [22, 23], in the context of active CD16⁺ NK cells, these cells may be depleted by ipilimumab (IPI) through antibody-dependent cellular

cytotoxicity (ADCC) [24]. We, therefore, hypothesized that enhanced ADCC function of the CIML NK cells in combination with IPI would mediate additional Treg depletion, leading to further enhanced CIML NK cell-mediated activity in the context of head and neck cancer. We observed that the addition of IPI was associated with contraction of Treg: Tcon in the peripheral blood lymphocyte compartment and promoted the expansion of mature and thus more cytotoxic NK cells early after adoptive transfer, but was also associated with more rapid NK cell rejection, thus acting as a “double-edged sword”. We posit that our findings will serve to guide future efforts aimed at combining NK cell-based approaches with other novel immunomodulatory agents.

Results

Adoptive transfer of haploidentical donor-derived CIML NK cells was safe and associated with transient disease control

This phase I clinical trial involved the infusion of haploidentical donor-derived CIML NK cells expanded and activated in vivo with N-803 following a course of lymphodepletion with fludarabine and cyclophosphamide. After completing the safety lead-in phase ($n=6$), the subsequent patients ($n=4$) also received a single dose of IPI (3 mg/kg) on day -7 as a means to further enhance donor NK cell activity (hypothesized to occur via Treg depletion) (Fig. 1a). Altogether, eleven patients with head and neck cancer refractory to a median of 6 lines of prior therapy, including 8 patients with oropharyngeal primaries, were enrolled, and 10 patients received donor CIML NK cells (one patient died from disease progression before CIML NK cell infusion) (Fig. 1b & Supplementary Fig. 1). The baseline patient and infusion product characteristics, as well as responses, are detailed in Supplementary Table 1. Overall, the treatment was well tolerated, meeting the primary safety endpoint of the trial. The median NK cell dose infused was 8.71×10^6 cells/kg, with NK cells constituting a median of 98.5% of all infused lymphocytes (range: 90.4–99.3%). Among the first 3 patients in the cohort without IPI, one patient experienced septic shock secondary to pseudomonas infection leading to death and meeting criteria for a dose-limiting toxicity (DLT). An additional 3 patients were subsequently treated in the same cohort without IPI and no DLTs were observed. No DLTs were observed in the next cohort of patients treated with IPI. Among all the treated patients, lymphodepletion was associated with transient grade 3–4 pancytopenia, with peripheral blood counts recovering at a median of 13 days after CIML NK cell infusion. Five patients developed mild (grade 1–2) cytokine release syndrome (CRS) and responded to tocilizumab (Table 1).

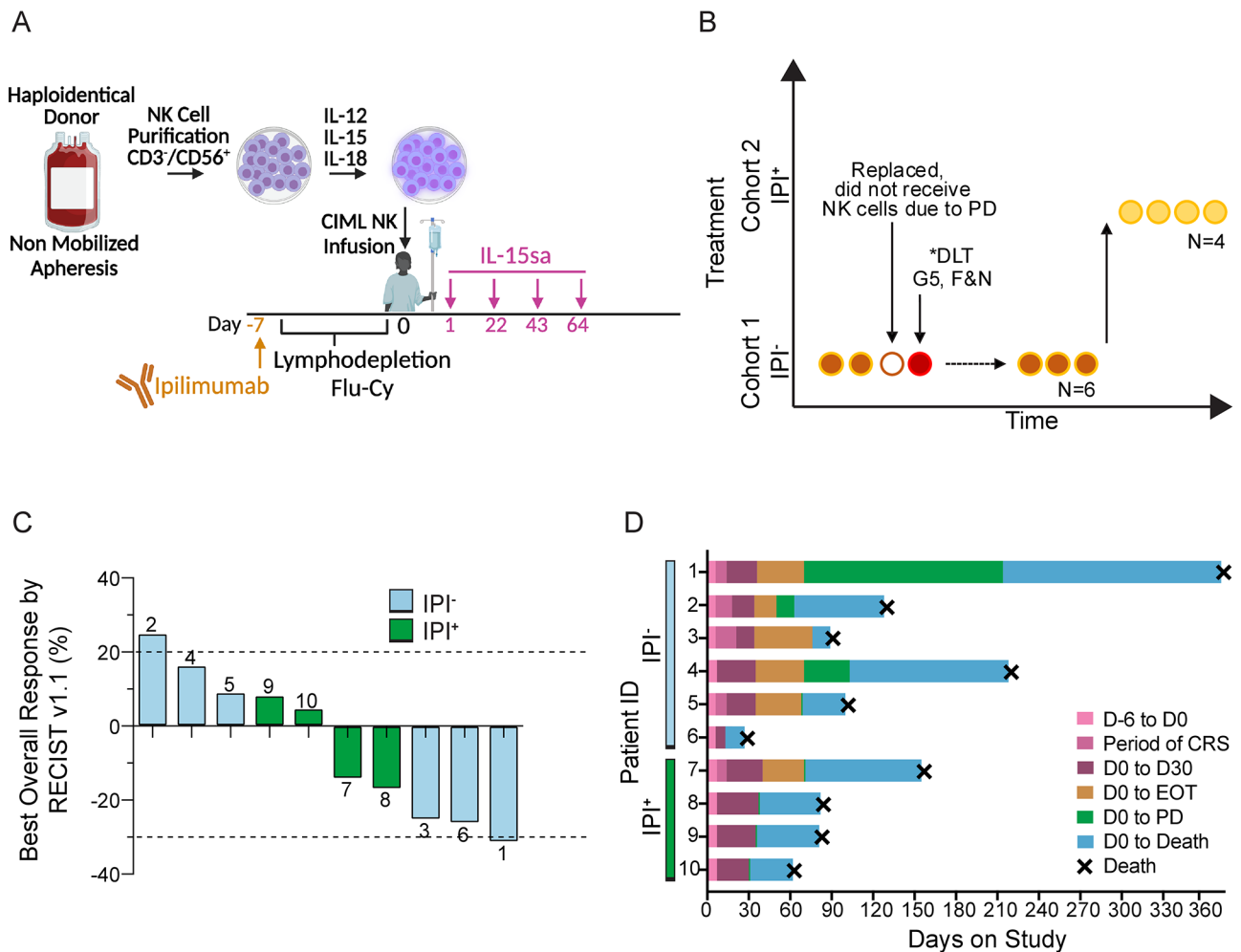


Fig. 1 Clinical outcomes of patients with relapsed/refractory head and neck cancer treated with haploidentical donor-derived CIML NK cell therapy. **A** Clinical trial schema describing CIML NK cell infusion product generation and trial therapy. For each patient, a haploidentical donor underwent non-mobilized apheresis of peripheral blood followed by CD3 depletion and CD56 positive selection. The product was then incubated in a cocktail of IL-12, IL-15, and IL-18 for 12–16 h to induce CIML differentiation and infused on day 0. The patients received lymphodepletion with fludarabine and cyclophosphamide, and IL-15 superagonist (IL-15sa) N-803 on day +1, with subsequent doses given every 3 weeks (up to 4 doses). After the first 6 treated patients were evaluated for safety, the subsequent patients also received a single dose of ipilimumab (IPI) 1 mg/kg on day –7 prior to starting lymphodepletion (created using Biorender). **B** Flow of the clinical trial. Cohort 1 in orange: (no IPI) DL0: $5-10 \times 10^6$ cells/kg. One patient was replaced (empty circle) due to NK cells not being received. Cohort 2 in yellow: (with IPI, 3 mg/kg \times 1) DL0: $5-10 \times 10^6$ cells/kg. *The patient with grade 5 adverse event of F&N (febrile neutropenia) and dose-limiting toxicity (DLT) in Cohort 1 is shown in red. **C** Waterfall plot showing tumor response by RECIST v1.1 criteria on day +30 following NK cell infusion. The bars in blue represent the first 6 evaluable patients on the trial who did not receive IPI while the green bars represent IPI treated patients. The number above each bar represents the patient ID on the trial. The dashed lines indicate size thresholds per RECIST v1.1 criteria. **D** Clinical course of all evaluable treated patients. Numbers on the vertical axis represent patient ID on the trial. The horizontal axis refers to days on study from the time of first therapy. D0: the day of CIML NK cell infusion, D30: day +30 response evaluation time point, CRS: cytokine release syndrome, EOT: end of treatment, PD: progressive disease

Secondary endpoints on the trial included objective response rate (ORR), disease control rate (DCR), progression-free survival (PFS), and overall survival (OS). Ten patients were evaluable on day +30 following CIML NK cell infusion. Six patients (60%) had stable disease as the best response, and 1 (10%) patient attained a partial response by RECIST v1.1 criteria [25], with target tumor volume shrinking by 30% (Fig. 1c & Supplementary Table 1). This resulted in transient DCR 70% and ORR 10%. One patient had a malignant pleural effusion

with head and neck cancer cells detectable at the time of initiation of trial therapy that demonstrated the predominance of NK cells (88% of the lymphocyte compartment) on day +14 following CIML NK cell infusion and had no detectable malignant cells in the pleural fluid on day +28 (Patient 3, Supplementary Table 2). At a median follow-up of 20.2 months, the median progression-free survival (PFS) was 3.0 months (95%CI 1-3.9), with the median overall survival (OS) 3.6 months (95%CI 1-4.7) (Fig. 1d).

Table 1 Adverse events for patients enrolled on the phase 1 trial

Event term	Number of patients (%) N = 11‡			
Grade 3–5 AEs* regardless of attribution	11 (100%)			
AEs leading to treatment discontinuation	1 (9%)			
TRAEs** leading to death	1 (9%)			
TRAEs at a frequency > 20% or any grade 3–5	All	Grade 3	Grade 4	Grade 5
Respiratory disorder, infection	1 (9%)	0	0	1 (9%)
Anemia	10 (91%)	10 (91%)	0	0
Decreased platelet count	8 (73%)	3 (27%)	2 (18%)	0
Nausea	8 (73%)	1 (9%)	0	0
Constipation	7 (64%)	0	0	0
Fatigue	7 (64%)	0	0	0
Decreased neutrophil count	6 (55%)	2 (18%)	3 (27%)	0
Decreased lymphocyte count	6 (55%)	0	5 (45%)	0
Fever	6 (55%)	0	0	0
Hypoalbuminemia	6 (55%)	0	0	0
Hypertension	5 (45%)	3 (27%)	0	0
Anorexia	5 (45%)	2 (18%)	0	0
Dyspnea	5 (45%)	1 (9%)	0	0
Decreased white cell count	5 (45%)	0	5 (45%)	0
Cytokine release syndrome	5 (45%)	0	0	0
Diarrhea	5 (45%)	0	0	0
Vomiting	5 (45%)	0	0	0
Dysphagia	4 (36%)	2 (18%)	0	0
Hypothyroidism	4 (36%)	0	0	0
Elevated alkaline phosphatase	4 (36%)	0	0	0
Elevated aspartate aminotransferase	4 (36%)	0	0	0
Hyperglycemia	4 (36%)	0	0	0
Hypophosphatemia	4 (36%)	0	0	0
Hypotension	4 (36%)	0	0	0
Febrile neutropenia	3 (27%)	3 (27%)	0	0
Hypoxemia	3 (27%)	3 (27%)	0	0
Dry mouth	3 (27%)	0	0	0
Hyponatremia	3 (27%)	0	0	0
Generalized pain	3 (27%)	0	0	0
Sinus tachycardia	3 (27%)	0	0	0
Cough	3 (27%)	0	0	0
Acute kidney injury	2 (18%)	1 (9%)	0	0
Back pain	1 (9%)	1 (9%)	0	0
Facial edema	1 (9%)	1 (9%)	0	0
Oral mucositis	1 (9%)	1 (9%)	0	0
Tumor bleeding	1 (9%)	1 (9%)	0	0

‡N = 11 patients who were enrolled on the study and started lymphodepleting chemotherapy, but only 10 patients received CIML NK cells because one patient had evidence of disease progression during lymphodepletion. The table shows percentages calculated out of a total of 11 enrolled patients

*AE: adverse events, **TRAE: treatment-related adverse events, †grading by CTCAE v5.0 criteria

There was no difference in PFS or OS between IPI treated and untreated patients (Supplementary Fig. 1).

Adoptive transfer of CIML NK cells followed by N-803 resulted in expansion and persistence of donor NK cells

We performed an in-depth evaluation of peripheral blood mononuclear cells following donor CIML NK cell infusion using a combination of multimodal assays from longitudinally banked samples (Fig. 2A). Adoptively transferred CIML NK cells expanded (increased their proportion of the total lymphocyte compartment by a minimum of 2-fold relative to the baseline trial screening time point within 14 days of NK cell infusion) in 8 of 10 patients, constituting a median of 85% (range: 34–98%) of all lymphocytes on day +7 versus 14% (range: 2–29%) at the trial screening time point (Fig. 2B & Supplementary Fig. 2A). Patients 2 and 8 did not have NK cell expansion at any evaluable time point, with the latter patient noted to have a donor-specific anti-HLA antibody (Supplementary Table 3). On day +14, the NK cells constituted a median of 70% (range: 1–92%) of the lymphocyte compartment in the patients with NK cell expansion (Fig. 2B). The median absolute NK cell counts at the time of screening (prior to CIML NK cell infusion), on day +7 and on day +14 were 77/uL, 208/uL, and 339/uL, respectively. NK cell expansion correlated with tumor volume reduction (Supplementary Table 4), with a higher fold expansion of the NK cell compartment (as absolute counts or percentage of lymphocytes) following infusion associated with a greater decline in tumor volume by RECIST v1.1 criteria ($R = -0.78$) (Fig. 2C, Supplementary Fig. 2B). Associations between responders to therapy and specific subpopulations of NK cells that expanded after infusion, based on tumor volume reduction as assessed at the trial response time points, are shown in Supplementary Table 4. Donor NK cell persistence between days 7–14 following CIML NK cell infusion was confirmed by both flow cytometry by gating on mismatched HLAs, and by DNA-based chimerism assay employing next-generation sequencing (Fig. 2D). The NK cell compartment contracted to pre-infusion levels by day +28 in 8 of 10 patients (Fig. 2B), concurrent with a loss of donor chimerism, while 2 subjects displayed donor NK cell persistence beyond day +28 (Fig. 2D). There was a trend toward greater expression of IFN γ following in vitro cytokine stimulation by day +14 following donor CIML NK cell infusion, consistent with the memory-like phenotype of these cells (Fig. 2E).

NK cell expansion and persistence were characterized by early proliferative and later mature activated phenotypes

While NK cells were the dominant cell type in the lymphocyte compartment until day +14, CD8⁺ T cells reconstituted and replaced the NK cells as the dominant

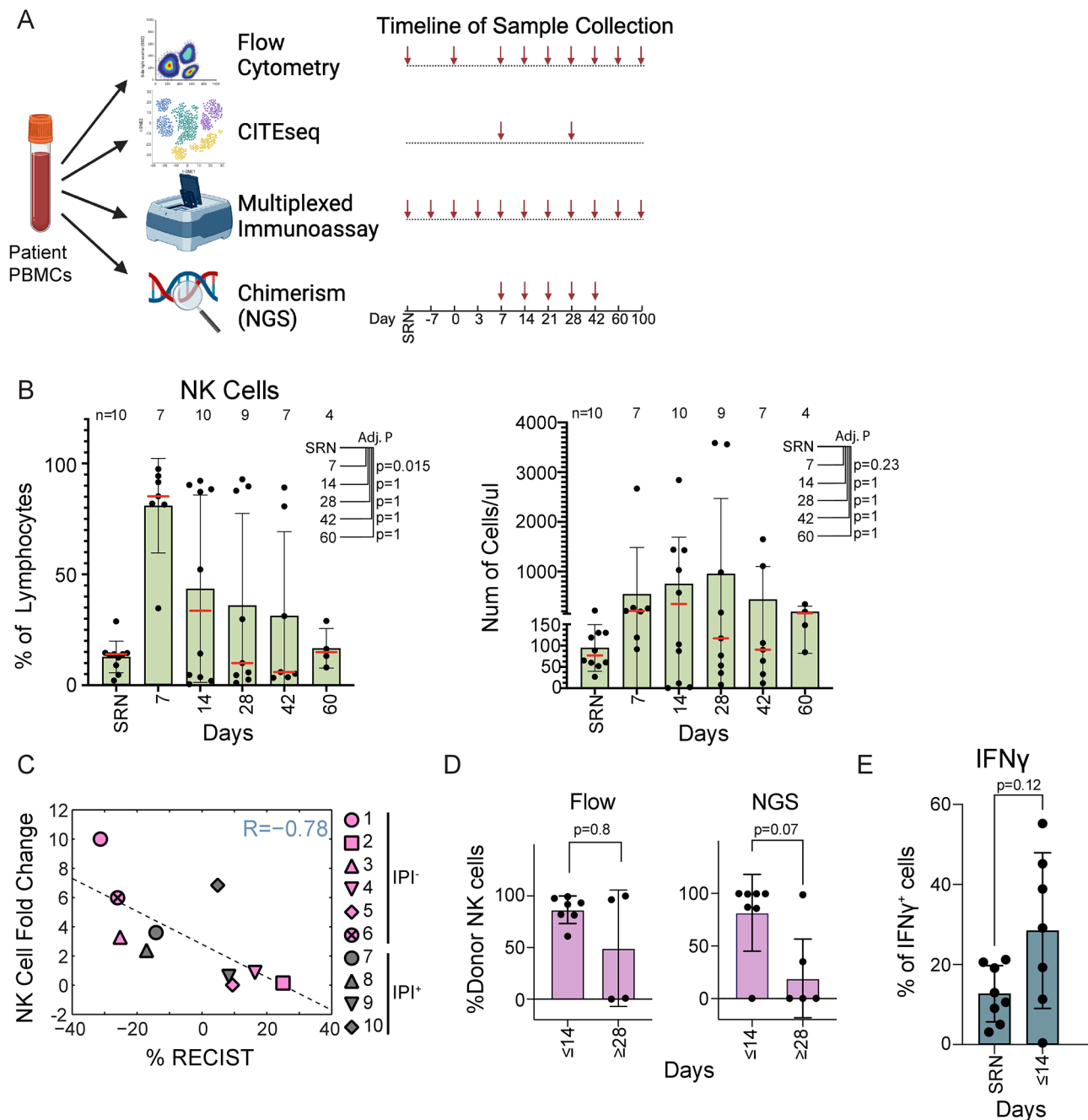


Fig. 2 (See legend on next page.)

lymphocyte type by day +28 (Fig. 3A). We evaluated the immunophenotype of the NK cells in the peripheral blood over time following CIML NK cell infusion by flow cytometry, using a customized NK cell panel (Supplementary Table 5). Within the NK cell compartment, the majority were CD56^{dim} at all assessed time points, although the CD56^{bright} NK subset appeared to expand beyond day +14 (Fig. 3B) [26, 27].

To evaluate the proteomic and transcriptional profiles of the total NK cells and study their potential interactions

with other immune cells in vivo at single-cell resolution, we performed single cell CITE-seq, which combines single cell RNA sequencing with a custom oligonucleotide tagged antibody panel (Fig. 3C & Supplementary Table 6) [28]. We found that NK cells underwent a transcriptional and immunophenotypic shift following their in vivo expansion (Fig. 3D). On day +7, gene set enrichment analysis showed evidence of NK cell proliferation (MYC_TARGETS_V1) (Fig. 3E) as well as a signature of NK activation (i.e. *JUN*, *JUNB*, *FOS*, *FOSB*, *GZMB*, and *PRF1*;

(See figure on previous page.)

Fig. 2 Expansion of the NK cells following donor cell product infusion. **A** Longitudinal evaluation of peripheral blood mononuclear cells (PBMCs) using flow cytometry with a customized panel, single-cell CITE-seq, a multiplexed immunoassay for secreted molecules, and next-generation sequencing of donor chimerism. The number of samples used for each assay at each time point is indicated (created using Biorender). **B** Size of the NK cell compartment as a proportion of total lymphocytes (left) and as absolute numbers (right) at the indicated time points after donor CIML NK cell infusion. Number of evaluable samples at each time point is shown above each bar. Adjusted p-values are determined using nonparametric Anova (Kruskal-Wallis test) followed by Dunn's multiple comparisons test. Shown are mean with SD, medians are marked by a red line. **C** Spearman correlation between NK cell expansion and tumor responses by RECIST v1.1 criteria. NK cell fold change was calculated by taking the ratio of NK cells as a percentage of lymphocytes, in the peripheral blood on day 14 following CIML NK cell infusion to the percentage of NK at the time of screening. The patient ID is indicated at each point. **D** Donor cells as a proportion of all peripheral blood mononuclear cells at the indicated time points using two different assays. Flow cytometry-based evaluation (Flow) using anti-HLA antibodies targeting recipient-donor disparity in HLA. DNA-based chimerism using next-generation sequencing (NGS) performed by CareDx was also used to evaluate donor chimerism. ≤ 14 ($n=7$) refers to available samples collected between day +7 and day +14, ≥ 28 ($n=4$ for Flow, $n=5$ for NGS) refers to available samples collected between day +28 and day +60. **E** Percentage expression of interferon gamma (IFN γ) in flow cytometry-based NK cell functional assays using live donor CD3⁻CD56⁺ lymphocytes (gated with donor-specific HLA antibodies) collected at the indicated time points following CIML NK cell infusion. In one recipient there was no donor-specific HLA antibody for flow cytometry gating, but the NGS-based chimerism confirmed that the NK cells were all donor, so the percentage was calculated on total NK cells. p-value for the comparisons in D, E were calculated using Mann-Whitney U. SRN: screening time point for the trial before NK cell infusion

Fig. 3F & Supplementary Table 7). Furthermore, gene expression representative of CD56^{bright} (*CD44*), adaptive (*CD3 ϵ* , *IL32*), and mature CD56^{dim} (*GZMB*, *NCR3*) NK cells were present (Supplementary Fig. 3) [27]. In contrast, the patterns of gene expression on day +28 were consistent with the presence of predominantly mature CD56^{dim} NK cells (Supplementary Fig. 3), with the expression of transcripts associated with NK cell activation [29] (Fig. 3E) and NK cell inhibitory receptors (i.e. *KIR3DL1*, *NKG2A*, and *KLRB1*; Fig. 3E, Supplementary Fig. 4 & Supplementary Table 7).

The *MKI67* gene was among the most differentially expressed in NK cells on day +7 compared to day +28. Other genes most highly expressed on day +7 included vimentin (*VIM*), stathmin 1 (*STMN1*), and tubulin (*TUBA1B*) -- all involved in cytoskeletal regulation and mitotic cell cycle (Supplementary Fig. 5) [30]. There was a minimal expression of genes associated with exhaustion of immune effector cells, characterized by genes such as *HAVCR2* (*Tim-3*) and *PDCD1* [31]. NK cells at all times expressed activating receptors, including *KLRK1*, *NKp30*, and *NKp46*. Concurrently, the largest concentration of known NK cell ligands for the expressed receptors was observed on the monocyte clusters (Supplementary Fig. 4F). The TGF β signaling pathway was upregulated in NK cells on day +28, compared to day +7 (Fig. 3E), characterized by the expression of *JUNB*, *HIPK2*, and *ID2* (Supplementary Fig. 6). Other key genes more highly expressed in NK cells on day +28 included the NK inhibitory receptor *KLRB1*, as well as *ZFP36*, *TXNIP*, and *SPON2* involved in cytokine responses and regulation as well as inflammatory cellular stress (Supplementary Fig. 5) [32, 33, 34].

Pseudotime analysis suggested two distinct differentiation trajectories of the infused NK cells (Fig. 3D): on day +7, one of these trajectories led to a CD16^{lo} NK cell population characterized by an upregulation of cell cycle genes (Supplementary Fig. 7) and proliferation (Fig. 3F), while the other trajectory led to a CD16^{hi} population

of predominantly mature CD56^{dim} NK cells expressing markers of NK activation concurrent with a gene expression signature comprised of NK inhibitory receptors (Fig. 3F & Supplementary Fig. 7). Upregulation of the chemokine genes *CCL3* and *CCL4*, and a chemotaxis gene signature characterized by the integrin receptor subunit genes *ITGA1* and *ITGA2* were also noted as the NK cell differentiated following infusion (Supplementary Fig. 8) [35].

Distinct patterns of secreted molecules were associated with NK cell expansion and concurrent changes in the tumor burden

We sought to evaluate the secretory molecule milieu to determine whether these molecules supported NK cell expansion and persistence and correlated with tumor burden reduction. Using a panel of 92 markers (Supplementary Table 8) applied to longitudinally collected plasma samples, we found distinct patterns of secreted molecules following NK cell infusion (Supplementary Fig. 9A). Endogenous soluble IL-15 levels (without measurement of N-803) were increased early after CIML NK cell infusion, concurrent with the period following lymphodepletion (Fig. 1A & Supplemental Fig. 9B) [36]. IL-6 levels were also concurrently increased, coinciding with the clinical development of CRS (though mild in all cases) in treated patients (Fig. 1D & Supplementary Fig. 9B). Endogenous IL-2 levels remained undetectable throughout the trial in all treated patients (data not shown). Increased plasma concentrations of CXCL10, *CCL3*, and *CCL4* also coincided with the period of NK cell expansion. The concentration of IFN γ and Granzyme B in the plasma of all treated patients was increased by day +7 and gradually decreased by day +28, concordant with the pattern of donor NK cell chimerism (Supplementary Fig. 9B). There was no correlation between the plasma concentrations of IL-12, IL-15, IL-18, *GZMB*, or IFN γ with the change in tumor burden following CIML NK cell infusion. (Supplementary Table 9).

The addition of ipilimumab was associated with increased NK cell proliferation, but an earlier contraction of the NK cell compartment following donor CIML NK cell infusion

To investigate the impact of IPI on immune reconstitution, we evaluated NK and T cell populations longitudinally and compared IPI non-treated (IPI⁻) and treated (IPI⁺) patients in this trial. The NK cell compartment as a proportion of total lymphocytes by day+14 was not different between IPI⁻ and IPI⁺ groups (Fig. 4A), but treatment with IPI was associated with a trend toward more rapid absolute NK cell expansion ($p=0.06$) (Supplementary Fig. 10), and a relative increase in mature CD16⁺CD57⁺KIR⁺ NK cells by day+14 (cluster 1 in Supplementary Fig. 11 & Supplementary Table 10). However, at the same time, IPI was associated with an earlier contraction of the NK cell compartment, with more rapid recovery of CD8⁺ T cells by day+28 in these patients (Fig. 4A). Furthermore, a comparison of peripheral blood mononuclear cell populations on days+7 and +28 based on single cell CITE-seq showed that the IPI treatment associated with persistence and earlier recovery of T cell and monocyte populations (Fig. 4B). Cell populations segregated as distinct populations on days+7 and +28 based on exposure to IPI treatment (by UMAP), suggesting that peripheral blood CD16^{hi} NK cells were depleted in the IPI⁺ patients (Fig. 4C).

Regarding the impact of IPI treatment on NK functional states, no clear association was observed (Supplementary Fig. 12). However, the use of IPI was associated with the expression of transcripts of receptors that may regulate NK cell effector function, including *KIR3DL1*, *KLRD1*, *KLRC1*, *HAVCR2*, and *ITGAL/LFA-1* (Supplementary Fig. 13 and Supplementary Tables 11 & 12). IPI was also associated with the upregulation of several key genes on day+7 that included proliferative gene sets in NK cell populations (Fig. 4D).

Ipilimumab treatment was associated with a decreased Treg: Tcon ratio and increased reconstitution of activated CD8 + T cells

To determine how adoptively transferred NK cells may interact with recipient T cells in mediating their effects and how IPI may potentially affect this interaction, we evaluated T cell reconstitution in all trial patients. Both CD4⁺ Tcon and CD8⁺ T cells were depleted on day+7 in all patients, with relative persistence of Treg (Fig. 5A). CD8⁺ T cells exhibited recovery on day+14 and became the dominant T cell population by day+28, with most having the central memory phenotype (Supplementary Fig. 14). A comparison of PBMC populations on days+7 and +28 with CITE-seq was consistent with the flow cytometry data, further showing distinct T cell clusters between the two time points. At the earlier time point, T cell clusters were predominantly double negative (DN)

T cells and Tregs, while at the later time point, they were predominantly CD8⁺ and CD4⁺ Tcons (Supplementary Fig. 14 & Fig. 3C). Mirroring the findings in NK cells, the day+7 time point was associated with the upregulation of proliferative pathways in T cells by GSEA while the day+28 time point was associated with an upregulation of inflammatory pathways, suggesting a state of T cell activation (Fig. 5B) [37].

Since IPI was added to potentially deplete CTLA4⁺ Tregs in the context of donor memory-like NK cell infusion, we compared Treg reconstitution in the IPI⁻ and IPI⁺ contexts. We found that the IPI⁺ context had a trend toward relative reduction in Treg: Tcon on day+14 following CIML NK cell infusion (Supplementary Fig. 14). On gene expression analysis, the TNF α signaling via NF κ B pathway, which plays a role in enhancing costimulatory signaling to the T cells [37], was particularly associated with the IPI⁺ context (Fig. 5C). Exhaustion markers such as *TIGIT*, *LAG3* and *HAVCR2* were most notable in the DN T cell population. While some CD8⁺ and CD4⁺ Tcon expressed *LAG3* on day+28, most of these cells did not express exhaustion markers (Fig. 5D).

Use of ipilimumab was associated with MHC-I signaling interactions between NK and T cells

To explore whether the reconstituting T cell populations on both day+7 and day+28 exhibited evidence of cross-talk with the NK cells and to evaluate the potential effects of the NK cell populations on reconstituting immune effector cells in the presence of N-803 and IPI, we conducted an interaction analysis using CellChat [38]. In the absence of IPI, the CD16^{lo} NK cells, which constituted the majority of NK cells on day+7, had relatively few predicted cell-cell interactions with T cells in contrast to the CD16^{hi} NK cells (Supplementary Fig. 15A). However, in the presence of IPI, far more predicted cell-cell interactions were detected between CD16^{lo} and CD16^{hi} NK cells and other immune effector cells (Supplementary Fig. 15A). Prominent among these interactions was that of the NK inhibitory receptor *KLRB1* (gene for CD161), which was among the most highly differentially expressed genes in NK cells on day+28 (Supplementary Fig. 5), and its ligand *CLEC2D* (gene for LLT1) on CD4⁺ Tcons, CD8+ T cells, Tregs, and several other cell populations (Supplementary Fig. 16). Other potential interactions between T cells and NK cells were in the CCL axis (Supplementary Fig. 17), with *CCL3* and *CCL4* gene expression being predominantly in NK cells (Supplementary Fig. 18). The analysis also predicted cell-cell communication via the MHC-I signaling axis in the context of IPI treatment, which occurred between CD16^{hi} NK cells and CD4⁺ Tcons on day+7 (Supplementary Fig. 15B) but was predominantly driven by the interaction between CD8⁺ T cells and CD16^{hi} NK cells on day+28 (Supplementary

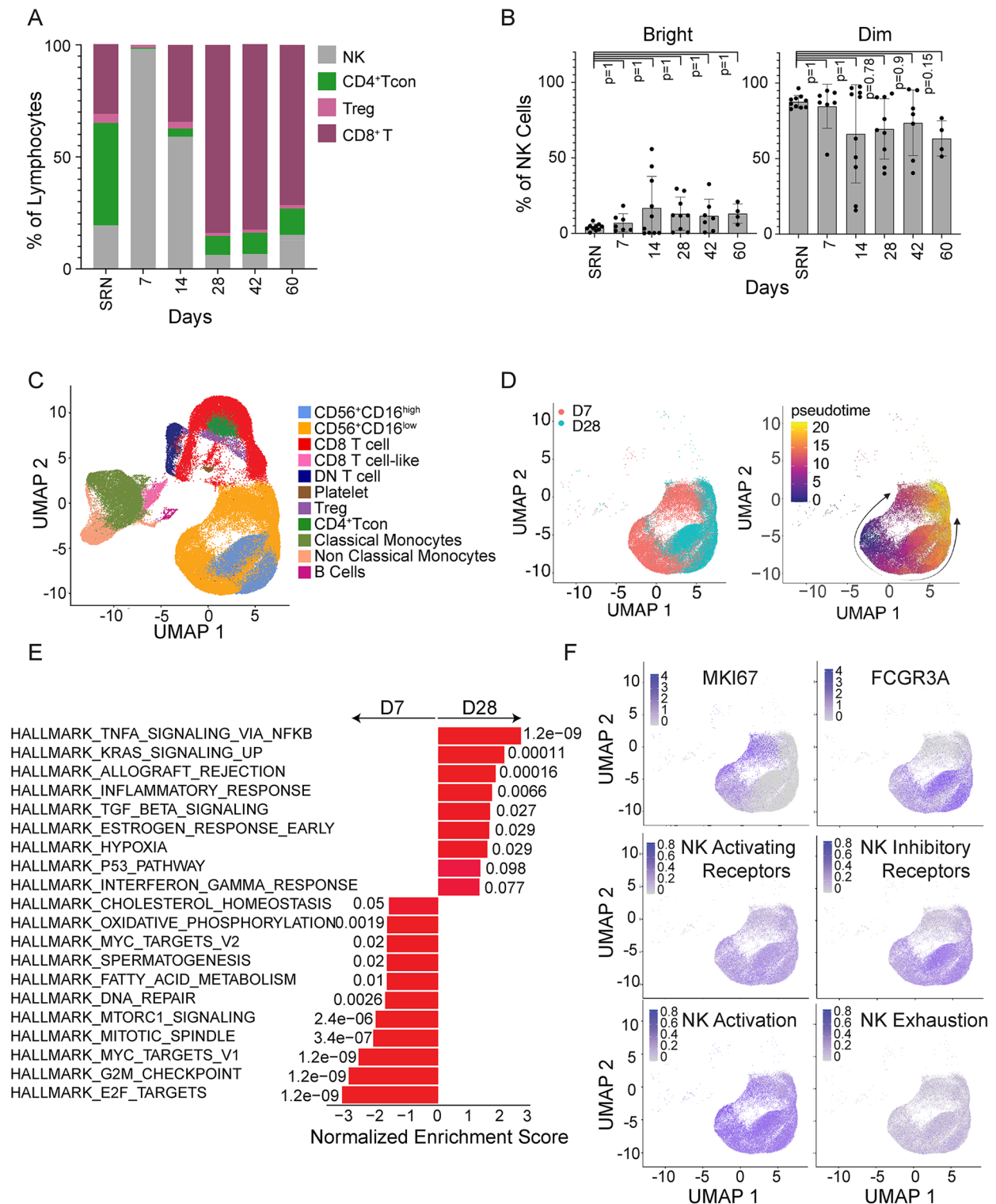


Fig. 3 (See legend on next page.)

Fig. 15C). The latter interaction was largely absent in the IPI⁻ patients, instead being largely driven by CD4⁺ Tcons. As the MHC-I signaling axis curated by the CellChat database mainly reflects interactions between the

CD8 receptor and HLA ligands [38], in the HLA mismatched context this would suggest CD8⁺ T cell-mediated rejection.

(See figure on previous page.)

Fig. 3 NK cell populations exhibit markers of proliferation and activation following CIML NK cell infusion. **A** Distribution of NK cells and T cells in the peripheral blood as a proportion of total lymphocytes assessed with flow cytometry. Data presented is a percentage of total lymphocytes. Gating strategies are indicated in Supplementary Fig. 19. **B** Distribution of the CD56^{dim} (Dim) and CD56^{bright} (Bright) NK cell population assessed with flow cytometry, mean and SD. Adjusted p-values for each time point comparison with SRN are determined using nonparametric Anova (Kruskal-Wallis test) followed by Dunn's multiple comparisons test. SRN: screening time point **C** UMAP of NK cell clusters defined using single cell CITE sequencing data, combining all patient samples ($n=4$) and all time points following CIML NK cell infusion (D7: day + 7, D28: day + 28). **D** Pseudotime plots demonstrating the differentiation trajectories of expanding NK cells. The plot on the left shows the same UMAP clustered by time. **E** Gene set enrichment analysis of pathways in NK cell clusters comparing days + 7 (D7) and + 28 (D28), with the earlier time point showing enrichment of proliferative gene sets while the latter time point showing enrichment of pathways associated with NK cell activation. **F** Expression of markers of proliferation (*MKI67*), *FCGR3A* (gene for CD16) and gene lists of NK activating receptors, inhibitory receptors, activation, and exhaustion. Key genes comprising these lists are described in the supplemental appendix (Supplementary Table 7). The intensity of expression is represented by the color in the legend within each plot

Discussion

We demonstrate that the combination of donor CIML NK cell infusion in combination with N-803 with or without IPI in patients with advanced relapsed/refractory head and neck cancer is safe and associated with transient disease control. The latter correlated with NK cell expansion. An in-depth multi-omic analysis allowed us to evaluate key phenotypic and gene expression changes in both the adoptively transferred NK cells and the recipient immune cell compartment. The addition of IPI was associated with decreased Treg: Tcon, increased activated CD8⁺ T cells, and a more rapid drop in the NK cells suggestive of enhanced rejection. We predicted novel immune cell-cell interactions which were further modulated by the addition of IPI. Overall, our findings highlight the broad impact of this innovative immunotherapy on multiple components of the immune cell compartment.

The addition of IPI in this trial stemmed from the hypothesis that it may induce antibody dependent cellular cytotoxicity (ADCC) targeting the CTLA4⁺ Tregs.²⁴ This phenomenon has been observed in mouse models, but it has not been definitively confirmed in human tumors [39], possibly due to species-specific differences in IgG isotypes and receptor expression. The intent was to start with one dose of the antibody that would result in its presence during CIML NK cell expansion, and to potentially further modify the dosing regimen in future iterations of the trial depending on the initial safety profile and outcomes. While IPI treatment was associated with a reduced Treg: Tcon ratio, possibly reflecting changes in both the Treg and Tcon subpopulations, and a more proliferative and activated NK cell phenotype in our study, it also correlated with a larger recipient CD8⁺ T cell compartment by day + 28 coinciding with a more rapid contraction of the peripheral blood donor NK cell compartment. Interestingly, a similar phenomenon has been observed with N-803 administered every 5 days in the context of another early phase trial using haploidentical CIML NK cells [40], whereby the authors hypothesized that increased sustained levels of systemic IL-15 led to the immunologic rejection of donor CIML NK cells by activated recipient CD8⁺ T cells. Whether IPI

administration leads to a similar phenomenon even at the lower total sustained concentration of systemic IL-15 expected with every 3-week administration of N-803 in our trial (as opposed to every 5-day in the aforementioned trial) is a hypothesis that requires further study.

While the donor NK cells persisted for a shorter period in the context of IPI, they did exhibit strikingly more predicted cell-cell interactions with other cells in the peripheral blood than in the IPI untreated patients. NK cells were the predicted receivers of immunomodulatory *CLEC* [41] signaling via *KLRB1* in the context of IPI, with the senders of the signal being primarily CD4⁺ Tcons. Additionally, CD8⁺ T cells and CD4⁺ Tcons were also the major receivers of signaling in the CCL axis, which in the context of increased secretion of CCL3 and CCL4 in the plasma during the period of NK cell expansion and gene expression of these chemokines in NK cells suggested that the latter were the senders of at least some of this signaling.

It is worth noting that CD16^{hi} NK cells were the predominant interacting partners with other immune effector cells based on CellChat analysis, both with and without IPI. Coupled with the observation that persistence of this subgroup of NK cells on FlowSOM analysis of flow cytometry data was associated with more tumor burden reduction as measured with RECIST v1.1 criteria, the enhanced cross-talk between these NK cells and other immune effector cells may play an important role in NK cell therapy. The interplay between the IL-15 α and IPI in the cross-talk between NK cells, other immune effector cells and tumor requires further study.

This study has important limitations. First, while we observe a correlation between donor NK cell expansion and tumor burden reduction, the number of treated patients is small. Furthermore, even though NK cells constituted the majority of the lymphocyte compartment in 7/10 patients, there was some heterogeneity in the absolute NK cell numbers in the peripheral blood in spite of all patients receiving similar NK cell product doses. In addition, due to the clinical status of the relapsed/refractory patients enrolled on the trial, biopsy of tumor following CIML NK cell infusion was not feasible, leading to a paucity of tumor tissue samples. This made it impossible

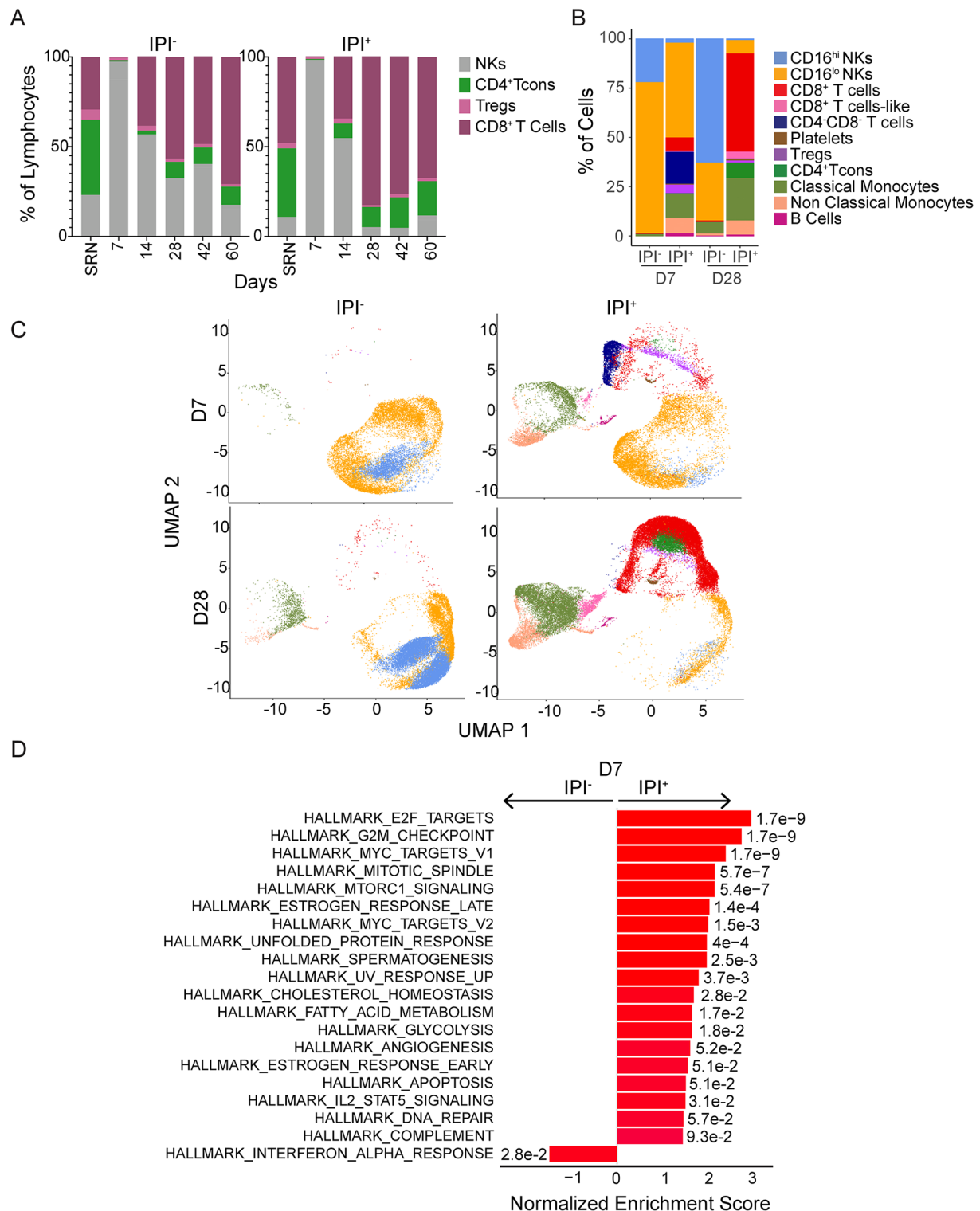


Fig. 4 Ipilimumab is associated with increased early NK cell proliferation but more rapid contraction of the NK cell compartment. **A** Distribution of NK cells and T cells in the peripheral blood as a proportion of total lymphocytes, stratified by IPI treatment, as evaluated with flow cytometry. The data presented is a percentage of total lymphocytes. **B** Distribution of peripheral blood mononuclear cells as measured with single cell CITE-seq on day +7 (D7) and day +28 (D28), comparing IPI treated (IPI⁺, *n*=2) and IPI untreated (IPI⁻, *n*=2) patients. **C** UMAP of NK cell clusters defined with single cell CITE-seq, separated by time points assessed and IPI treatment. The color scheme corresponds to the same populations as shown in **B**. **D** Gene set enrichment analysis of pathways in NK cell clusters comparing IPI⁺ (*n*=2) and IPI⁻ (*n*=2) patients on day +7 (D7)

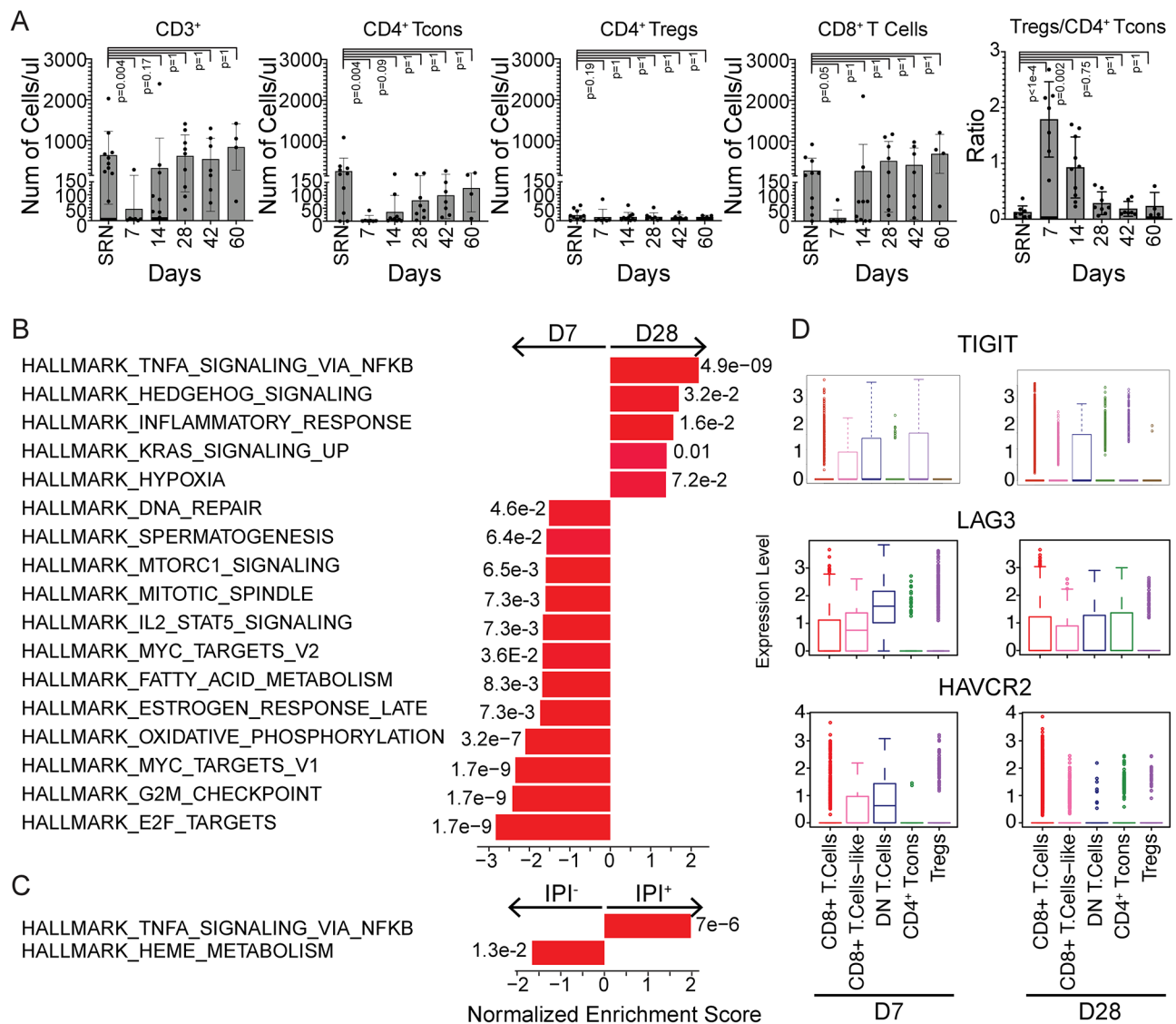


Fig. 5 T cell reconstitution following CIML NK cell infusion. **A** Distribution of the T cell populations assessed by flow cytometry, mean, and SD. Adjusted p-values for each time point comparison with SRN (trial screening time point) are determined using non parametric anova (Kruskal-Wallis test) followed by Dunn's multiple comparisons test. **B** Gene set enrichment analysis of pathways in T cell clusters comparing days +7 (D7) and +28 (D28), showing enrichment of pathways of activation at the latter time point. **C** Gene set enrichment analysis of pathways in T cell clusters comparing IPI untreated (IPI⁻) and treated (IPI⁺) conditions. **D** Expression of exhaustion markers in T cell populations on days +7 (D7) and +28 (D28). Boxplots show median and quartiles. Mann-Whitney U test. P-values were calculated per cell type and are detailed in Supplementary Table 15

to confirm whether the administration of IPI led to a reduction of CTLA4⁺ Tregs in the tumor microenvironment as hypothesized. Further studies will be needed to definitively confirm or reject this hypothesis. Although these limitations do not allow for simple generalizations of all the findings, the deep immunophenotypic and transcriptional analysis of longitudinal samples generated important hypotheses with potential for future clinical translation. The transient disease control observed in the study has prompted further amendments to the protocol, including the removal of lymphodepleting chemotherapy, extending the use of N-803 beyond day +100,

addition of the epidermal growth factor receptor inhibitor cetuximab, use of an off-the-shelf NK cell product that allows for repeated infusions (Clinicaltrials.gov ID: NCT06239220), and consideration of using an autologous CIML NK cells to prevent their rejection. Ongoing work aims to validate and better understand the mechanisms driving inferred interactions between donor NK cells and recipient immune effector cells to further optimize the efficacy of the memory-like NK cell platform.

In summary, we demonstrate that the haploidentical donor CIML NK cells in combination with N-803 with or without IPI treatment is safe and associated with

promising though transient disease control in patients with relapsed/refractory head and neck cancer. While IPI was associated with more proliferative and activated NK cells, it was also associated with shorter donor NK cell persistence possibly driven by CD8⁺ T cell-mediated allogeneic rejection.

Methods

Trial participants

This phase 1 single-center (Dana-Farber Cancer Institute), open-label, clinical trial enrolled patients with recurrent or metastatic (R/M) head and neck cancer (either head and neck squamous cell carcinoma [HNSCC] or salivary gland cancer) regardless of human papillomavirus (HPV) status who had received prior platinum and immunotherapy (anti-PD-1) treatments in the R/M setting (for the HNSCC patients, specifically); with no restrictions of number of lines of prior therapy. Patients 18 years of age or older with any smoking history were eligible if their ECOG performance status was 2 or less and they had measurable disease (RECIST v1.1). The trial was approved by the DF/HCC institutional review board (IRB) (19–505), conducted in accordance with the Declaration of Helsinki and Good Clinical Practice Guidelines, and registered nationally (NCT04290546). CIML NK cell product generation from related haplo-identical donors was performed as previously described [12]. All donors were evaluated by a medical team independent of the trial investigators, and provided consent for donation on the clinical trial as per standard institutional operating procedure. All CIML NK cell products met clinical trial release criteria that included: total cell viability $\geq 70\%$, NK cell (CD3⁻CD56⁺) fraction $\geq 70\%$ of viable leukocytes, and T cell (CD3⁺) content $< 3.0 \times 10^5$ cells/kg.

Study design

Patients in cohort 1 received lymphodepleting chemotherapy with fludarabine (25 mg/m²/day) for 5 days starting on day -6 and cyclophosphamide (50 mg/kg/day) for 2 days starting on day -5 prior to haplo-identical CIML NK cell infusion on day 0 ($5\text{--}10 \times 10^6$ viable cells/kg = dose level 0) followed by N-803 (IL-15 superagonist [IL-15sa], 15 mcg/kg subcutaneously) starting on day +1 every 21-days for 4-doses. In cohort 2, patients received the same regimen with a dose of lead-in ipilimumab (3 mg/kg IV) on day -7. Cohort 1 treated 3 patients at dose level 0 (adhering to a 3+3 dose de-escalation design); < 2 DLTs triggered an additional 3 patients ($n=6$). Cohort 2 treated an additional 4 patients. The primary study objectives were to establish safety and tolerability and to estimate the maximum tolerated dose (MTD) of CIML NK cells. Secondary objectives were to characterize the objective response rate (RECIST v1.1)

to therapy at day +30 (4 weeks) and day +84 (12 weeks) following CIML NK cell infusion, to estimate progression-free survival (PFS) and overall survival (OS), and to determine the phenotypic expansion and function of adoptively transferred NK cells with correlation to clinical benefit and survival. Data as of December 17, 2023, were analyzed. Deidentified clinical data that can be shared in accordance with institutional policy is available upon request from Dr. Glenn Hanna.

Patient and healthy donor samples

Patients provided written informed consent prior to participation under an IRB-approved protocol at the Dana-Farber Cancer Institute where all protocol procedures were performed and data were collected. Correlative samples included peripheral blood collected at screening for the trial, on day -7 (before starting lymphodepletion), day 0, day +7, day +21–28, day +42, day +60, day +100, and relapse time points after infusion. Samples acquired from patients for the purpose of all correlative studies cannot be obtained again from the same patients. Healthy donor PBMCs (peripheral blood mononuclear cells) were isolated by Ficoll centrifugation, and NK cells were purified using EasySep (STEMCELL Technologies, 17955). All PBMCs were cryopreserved according to a standard internal laboratory protocol at the time of collection from patients. Exclusion of any collected samples from planned correlative studies was only done if the cell viability was poor or cell quantity was insufficient. Due to the clinical status of the heavily pretreated patients enrolled on this trial, collection of tumor biopsy samples for research purposes following CIML NK cell infusion was not feasible.

Flow cytometric analysis

A custom NK and T cell panel of antibodies was used (Supplementary Table 5). All cell staining for flow cytometry was performed as previously described [10], and data were acquired on a BD LSR Fortessa flow cytometer and analyzed using FlowJo (Tree Star) software. Gating strategies for NK cells and T cells are shown in representative plots (Supplementary Fig. 19). The absolute lymphocyte count was measured using a clinical assay. For any lymphocyte population not measurable directly with the clinical assay, the absolute count of this population was determined by multiplying its percentage (percent of total lymphocytes) as measured with flow cytometry by the total lymphocyte count measured at the same time point using the clinical assay. For one patient we used day 21 sample instead of day 28 which was not available.

Olink cytokine assays

Serum from the patients were analyzed for 96 protein biomarkers using the Olink Target 96 Immuno-Oncology

panel (Supplementary Table 8). Olink proteomics is based on a proximity extension assay, where oligonucleotide-labeled antibody probe pairs are allowed to bind to their respective targets in the sample in 96-well plate format. The quality control was performed using Olink® NPX Signature software, and additional QC was performed by removing seven poorly detected proteins from further analyses. Data are presented as log₂-transformed units NPX. Higher NPX values correspond to a higher protein expression. Spearman correlation was used to detect cytokines associated with response.

Functional and flow-based cytotoxicity assays

Frozen PBMCs were thawed and cultured overnight in RP10 medium (RPMI 1640 supplemented with 10% FBS, 1× penicillin/streptomycin, 2mM L-glutamine, and 7.5 mmol HEPES) with 1ng/mL IL-15. K562 cells were cultured in RP-10 medium and labeled with 5 μm of CellTrace Violet (Thermo Fisher Scientific) in PBS for 20 min at 37 °C and washed with RP10. To measure HLA donor chimerism, intracellular IFN γ and degranulation, cells were stained as follows: PBMCs, PBMCs with cytokines (IL-12 10ng/ml, IL-18 50ng/ml, IL-15 50ng/ml), or PBMCs with K562 cells at 10:1 E: T ratios, were co-cultured for 1 h, followed by the addition of 0.2uL BD GolgiPlug™ (BD Biosciences), 0.13uL BD GolgiStop™ (BD Biosciences) and 1uL of APC-CD107a (Biolegend). After an additional 5 h of co-culture, cells were stained for extracellular proteins with CD56, CD3, CD16, HLA antibodies (Supplementary Tables 5, 13) and violet live-dead stain (thermos fisher, 1:1000). Intracellular staining for IFN γ was performed using BD Cytofix/Cytoperm (BD Biosciences). Cells were acquired using BD LSR Fortessa and analyzed using FlowJo (Tree Star). Data is presented selectively for donor NK cells, based on the staining of HLA.

Donor chimerism

The assessment for the persistence of the donor CIML NK cell therapy product in patient samples was performed using the AlloCell test (CareDx). NK cells were isolated from PBMCs using negative bead selection for CD56 (STEMCELLS technologies). Cell pellets were shipped to CareDx for AlloCell testing. Briefly, genomic DNA was extracted and measured by Qubit (Qubit™ Flex Fluorometer, Thermo Fisher Scientific) for quality control. A minimum of 8ng gDNA was used for targeted amplification of hundreds of single nucleotide polymorphisms (SNPs) in a single multiplex reaction on Mastercycler® Nexus Thermal Cycler (Eppendorf). Next Generation Sequencing (NGS) was performed on NextSeq 550 (Illumina). Percent cell product measurements were established by analyzing the relative contributions of SNP alleles with CareDx's proprietary AlloCell data

analysis pipeline incorporating open and custom bioinformatics tools. The results were reported as % Cell product relative to the patient genome.

The assessment for the persistence of the donor CIML NK cell therapy product in patient samples was also performed using flow cytometry evaluating HLA (Supplementary Table 13). Cells were stained for either donor or recipient as part of the functional assays described above.

Single-cell RNA-seq and CITE-seq sequencing and analysis

Cryopreserved PBMC samples from patients were thawed and diluted in RP10 media. Samples with low viability rates were enriched for live cells using dead cell removal (Annexin V) kit (STEMCELLS technologies). Cells were stained with CITE-seq antibodies (TotalSeq™-C Human Universal Cocktail, V1.0, BioLegend) per manufacturer's instruction, using 1:3 or 1:4 dilution of the antibody pool, supplemented with 2ul of each custom antibody. Briefly, 0.5-1 million cells were resuspended in 50uL cell staining buffer (PBS with 0.04% ultrapure BSA, #AM2616), 5uL of Human TruStain FcX Fc Blocking reagent (BioLegend) was added and the mixture was incubated for 10 minutes at 4°C. Following this, the CITE-seq antibody cocktail, adjusted to 50ul in staining buffer, was added and incubated for 30 minutes at 4°C. The mixture was then washed 3 times with 1 mL the staining buffer and resuspended in 1000 cells/uL. Single-cell libraries were prepared using the 10x Chromium Next GEM Single Cell 5' v2 Kit (10XGenomics), according to the manufacturer's instructions. The single-cell RNA-seq and CITE-seq libraries were sequenced by NovaSeq S4 flowcell (Illumina). Single-cell RNA-seq and Cite-seq data were processed, aligned to hg38, and aggregated using CellRanger (version 7.1.0) [42]. Cite-Seq and expression data were analyzed using Seurat (version 5.0.0) [43]. Data from individual samples was analyzed separately prior to combining the data from multiple samples. The outlier cells with a very low number of gene features (<200) or low total UMI (<500), or high number of gene features (>7000) were removed. Cells with a high mitochondrial ratio (>20%) from each data set were also filtered out. After filtering, individual samples were combined based on the identified anchors for the following integrated analysis. Principal component analysis (PCA) was performed and the first 10 principal components (PCs) were used to cluster cells using the Louvain algorithm in Seurat. These PCs were then used to run UMAP clustering. Well-defined marker genes for each cluster were used to identify potential cell populations [44, 45, 46], such as T cells (CD2, CD3D, CD3E, CD3G), Treg (RTKN2, FOXP3, CD4, IL2RA, TIGIT, CTLA4, FCRL3, LAIR2, IKZF2), B cells (IGLL5, MZB1, JCHAIN, DERL3, SDC1, MS4A1, BANK1, PAX5, CD79A), CD14⁺ monocytes (S100A9, CTSS, S100A8, LYZ, VCAN, S100A12,

IL18, CD14, G0S2, FCN1), CD16⁺ monocytes (CDKN1C, FCGR3A, PTPRC, LST1, IER5, MS4A7, RHOC, IFITM3, AIF1, HES4) and NK cells (NCAM1, KLRD1, KLRF1, NKG7, GNLY), platelets (PPBP, PF4, NRG1, GNG11, CAVIN2, TUBB1, CLU, HIST1H2AC, RGS18, GP9). Gene Signature enrichment analysis was performed with the R package AUCell (version 1.26) [47]. Differential gene expression analysis between scRNA-seq cell population was performed using the FindMarkers() function in Seurat package with logfc.threshold set to 0, expect for the results presented in Figure S7 where we used DESeq2 package (version 1.34.0) [48] and a pseudo-bulk approach with patients as replicates. Cell-cell interaction analysis was performed with CellChat package (version 1.6.1) [38] using the functions identifyOverExpressedGenes(), identifyOverExpressedInteractions(), computeCommunProb() with default parameters, filterCommunication() with min.cells set to 3, computeCommunProbPathway() and aggregateNet() with default parameters, and netAnalysis_computeCentrality() with slot.name set to "netP". Pseudotime analysis was performed on NK cell population using the learn_graph() function of Monocle3 package (version 1.3.4) [49] with default parameters. The pseudotime path was rooted with the node with the highest expression of TUBA1B (the gene with the lowest expression in D28 relative to D7). For pathways representing specific cellular functions, we performed Gene Set Enrichment Analysis using the Hallmark gene set collection [50] and ClusterProfiler (version 4.12) [51].

Statistical analyses

All flow cytometry data were tested for normal distribution (Shapiro-Wilk test), and if the data were not normally distributed, the appropriate non-parametric tests were used (GraphPad Prism v5.0). Differential expression of single-cell RNA sequencing data was performed using the Mann-Whitney U test as part of the Seurat package [43]. All statistical comparisons are indicated in the figure legends. All comparisons used a two-sided alpha of 0.05 for significance testing. All measurements were taken from distinct samples. All data for correlative studies and analysis is available upon request from the corresponding author.

Supplementary Information

The online version contains supplementary material available at <https://doi.org/10.1186/s13045-025-01669-3>.

Supplementary Material 1

Acknowledgements

We would like to thank M. Shipp (DFCI) for discussion and guidance, and D. Hearsey (DFCI) for assistance in processing and banking clinical samples. We are grateful to Miltenyi Biotec for providing materials for cell processing and product preparation. We are grateful to ImmunityBio for providing N-803, and

to BMS for providing IPI. We thank Allyson Moulton, BS, Evgeniya Vaskova, PhD Natali Gulbahce, PhD, Marica Grskovic, PhD, and the R&D lab at Cell Transplant Therapy, CareDx, Inc, for their assistance with planning, developing, performing and analyzing the results of the NGS-based chimerism assay used in this manuscript. We are grateful for the patient volunteers who gave their time and provided the samples for all correlative studies. We are also grateful to the cellular therapy and research coordinators at the Dana-Farber Cancer Institute.

Author contributions

RMS and MS contributed equally to the study. GH and RR designed the clinical study protocol. RMS, MS, and RR designed the correlative studies. SN prepared CIML NK products under good manufacturing practice (GMP) guidelines and was responsible for quality control of the products. GB, YZA, IEK, DK, MuT processed and prepared patient samples for correlative studies, and performed experiments. MS performed the NK cell functional assays. RMS, MS, ND, and AK planned and conducted NGS-based chimerism using patient samples. MA performed flow cytometry and RMS, MS, RD and MA analyzed the flow cytometry data. LP, RMS, and MS planned the single cell CITE-seq experiments. MS, MSF, JF, SL, and WL performed single-cell CITE-seq, and RMS, MS, MAB, and MYT performed data analyses. JB performed the Olink cytokine panel. GH recruited clinical trial participants. RMS and MS analyzed all the data and designed the figures. RMS, MS, GH, and RR interpreted the data and wrote the first draft of the manuscript. CJW, JK, RJS, RU and JR reviewed the manuscript and provided critical feedback on the results of the correlative studies. All authors revised the manuscript critically and approved the final version.

Funding

Gateway for Cancer Research, Ted and Eileen Pasquarello Research Fund, Goldfarb and Rudkin Family Fellowship, Dr. Antin's Research Fund, Massey Family Fund. MS is funded by the Sidney Farber Scholar Program, Dana Farber, and RR is a recipient of the Career Development Award from the Leukemia and Lymphoma Society and is a member of the Parker Institute for Cancer Immunotherapy at Dana-Farber Cancer Institute.

Data availability

Sequence data that supports the findings of this study will be deposited in an appropriate repository by the time of article publication. Data is available upon request.

Declarations

Ethical approval

This study was reviewed and approved by the institutional review board of the Dana-Farber Cancer Institute, Boston, MA, USA (Clinicaltrials.gov: NCT04290546). The study was performed in compliance with the provisions of the Declaration of Helsinki and Good Clinical Practice guidelines. Written informed consent was obtained from participants before inclusion in the study. Patients provided written informed consent to participate and to publish under an IRB-approved protocol at the Dana-Farber Cancer Institute where all protocol procedures were performed and data were collected.

Role of funding source

The funding source had no role in the design of this study, its execution, analyses, interpretation of the data, or decision to submit the results.

Competing interests

RD has received research funding from Ligue Contre le Cancer, Arthur Sachs, Monahan Foundation, Servier Foundation, Philippe Foundation, DCP AP-HP, honoraria from Novartis and Takeda, as well as non-financial support from Kite Pharma / Gilead and Sanofi. MSF receives funding from Calico Life Sciences, Bristol-Myers Squibb, Istari Oncology and served as a consultant for Galvanize Therapeutics. ND and AK are employees of CareDx. JK reports research support from Amgen, Equillium, BMS, Miltenyi Biotec, Regeneron, and Clinigen and consulting income from Amgen, Equillium, and Moderna Therapeutics, and is a scientific advisory board member for Cugene and Therakos. SN reports ad hoc advisory boards for Kite/Gilead, GlaxoSmith Kline, Iovance, A2 Bio and Sobi. JR receives research funding from Kite/Gilead, Novartis and Oncternal Therapeutics and serves in a consulting/advisory role for Garuda Therapeutics, LifeVault Bio, Smart Immune and TriArm Therapeutics.

CJW holds equity in BionTech, Inc; and receives research funding from Pharmacyclics. She is a member of the scientific advisory boards of Adventris, Aethon Therapeutics and Repertoire. RJS serves on the board of directors for Be The Match/National Marrow Donor Program; provided consulting for Vor Biopharma, Neovii, CSL Behring, Bluesphere Bio, Cugene, Jasper, Smart Immune; and is on the Data Safety Monitoring board for Juno Therapeutics. GJH receives grant funding to institution from: ACCRF, Actuate, Bicara, BMS, Coherus, Elevar, Gateway for Cancer Research, Genentech, ImmunityBio, KSQ, Kura Oncology, Regeneron, Remix, Replimune, and Secura Bio; and serves in a consulting/advisory role to: Bicara, Coherus, Inhibrx, Kura Oncology, Merck, Navaris, Nextech, OncoSwitch, Regeneron, and Replimune. RR receives funding from CRISPR Therapeutics, Skyline Therapeutics, and is on the advisory board of Glycostem.

Author details

¹Division of Transplantation and Cellular Therapies, Dana-Farber Cancer Institute, Harvard Medical School, Boston, USA

²Department of Informatics and Analytics, Dana-Farber Cancer Institute, Boston, USA

³Krantz Family Center for Cancer Research, Department of Medicine, Massachusetts General Hospital, Boston, USA

⁴Broad Institute of MIT and Harvard, Cambridge, MA 02142, USA

⁵Translational Immunogenomics Laboratory, Dana-Farber Cancer Institute, Boston, MA, USA

⁶Department of Clinical Hematology and Cellular Therapy, Sorbonne University, Saint-Antoine Hospital, Assistance Publique - Hôpitaux de Paris, Inserm UMRs 938, Centre de recherche Saint-Antoine, Paris, France

⁷Center for Immuno-oncology, Dana Farber Cancer Institute, Harvard Medical School, Boston, USA

⁸Cell Transplant Therapy, CareDx Inc, Brisbane, CA, USA

⁹Department of Surgery, Brigham and Women's Hospital, Boston, MA, USA

¹⁰Department of Data Science, Dana-Farber Cancer Institute, Boston, USA

Received: 18 November 2024 / Accepted: 2 February 2025

Published online: 14 February 2025

References

- Hanna GJ, Patel N, Tedla SG, Baugnon KL, Aiken A, Agrawal N. Personalizing surveillance in Head and Neck Cancer. *Am Soc Clin Oncol Educ Book*. 2023;43e389718. https://doi.org/10.1200/EDBK_389718.
- Ionna F, Bossi P, Guida A, et al. Recurrent/Metastatic squamous cell carcinoma of the Head and Neck: A big and intriguing challenge which May be resolved by Integrated treatments combining Locoregional and systemic therapies. *Cancers*. 2021;13(10). <https://doi.org/10.3390/cancers13102371>.
- Ferris RL, Licitra L. PD-1 immunotherapy for recurrent or metastatic HNSCC. *Lancet*. 2019;394(10212):1882–4. [https://doi.org/10.1016/S0140-6736\(19\)32539-5](https://doi.org/10.1016/S0140-6736(19)32539-5).
- Burtneß B, Harrington KJ, Greil R, et al. Pembrolizumab alone or with chemotherapy versus cetuximab with chemotherapy for recurrent or metastatic squamous cell carcinoma of the head and neck (KEYNOTE-048): a randomised, open-label, phase 3 study. *Lancet*. 2019;394(10212):1915–28. [https://doi.org/10.1016/S0140-6736\(19\)32591-7](https://doi.org/10.1016/S0140-6736(19)32591-7).
- Jung EK, Chu TH, Vo MC, et al. Natural killer cells have a synergistic anti-tumor effect in combination with chemoradiotherapy against head and neck cancer. *Cytotherapy*. 2022;24(9):905–15. <https://doi.org/10.1016/j.jcyt.2022.05.004>.
- Kilian M, Friedrich MJ, Lu KHN et al. The immunoglobulin superfamily ligand B7H6 subjects T cell responses to NK cell surveillance. *Sci Immunol*. 9(95):eadj7970. <https://doi.org/10.1126/sciimmunol.adj7970>
- Andrew J, Charap T, Enokida R, Brody, et al. Landscape of natural killer cell activity in head and neck squamous cell carcinoma. *J Immunother Cancer*. 2020;8(2):e001523. <https://doi.org/10.1136/jitc-2020-001523>.
- Jacobs MT, Wong P, Zhou AY, et al. Memory-like differentiation, Tumor-Targeting mAbs, and chimeric Antigen receptors enhance natural killer cell responses to Head and Neck Cancer. *Clin Cancer Res*. 2023;29(20):4196–208. <https://doi.org/10.1158/1078-0432.CCR-23-0156>.
- Romee R, Schneider SE, Leong JW, et al. Cytokine activation induces human memory-like NK cells. *Blood*. 2012;120(24):4751–60. <https://doi.org/10.1182/blood-2012-04-419283>.
- Romee R, Rosario M, Berrien-Elliott MM, et al. Cytokine-induced memory-like natural killer cells exhibit enhanced responses against myeloid leukemia. *Sci Transl Med*. 2016;8(357):ra357123–357123. <https://doi.org/10.1126/scitranslmed.aaf2341>.
- Gang M, Wong P, Berrien-Elliott MM, Fehniger TA. Memory-like natural killer cells for cancer immunotherapy. *NK Cell Immunother*. 2020;57(4):185–93. <https://doi.org/10.1053/j.seminhematol.2020.11.003>.
- Shapiro RM, Birch GC, Hu G, et al. Expansion, persistence, and efficacy of donor memory-like NK cells infused for posttransplant relapse. *J Clin Invest*. 2022;132(11). <https://doi.org/10.1172/JCI154334>.
- Berrien-Elliott MM, Foltz JA, Russler-Germain DA et al. Hematopoietic cell transplantation donor-derived memory-like NK cells functionally persist after transfer into patients with leukemia. *Sci Transl Med*. 14(633):eabm1375. <https://doi.org/10.1126/scitranslmed.abm1375>
- Bednarski JJ, Zimmerman C, Berrien-Elliott MM, et al. Donor memory-like NK cells persist and induce remissions in pediatric patients with relapsed AML after transplant. *Blood*. 2022;139(11):1670–83. <https://doi.org/10.1182/blood.2021013972>.
- Zhou Y, Husman T, Cen X, et al. Interleukin 15 in cell-based Cancer Immunotherapy. *Int J Mol Sci*. 2022;23(13). <https://doi.org/10.3390/ijms23137311>.
- Van der Meer JMR, Maas RJA, Guldevall K, et al. IL-15 superagonist N-803 improves IFN γ production and killing of leukemia and ovarian cancer cells by CD34+ progenitor-derived NK cells. *Cancer Immunol Immunother*. 2021;70(5):1305–21. <https://doi.org/10.1007/s00262-020-02749-8>.
- Romee R, Cooley S, Berrien-Elliott MM, et al. First-in-human phase 1 clinical study of the IL-15 superagonist complex ALT-803 to treat relapse after transplantation. *Blood*. 2018;131(23):2515–27. <https://doi.org/10.1182/blood-2017-12-823757>.
- Wrangle JM, Velcheti V, Patel MR, et al. ALT-803, an IL-15 superagonist, in combination with nivolumab in patients with metastatic non-small cell lung cancer: a non-randomised, open-label, phase 1b trial. *Lancet Oncol*. 2018;19(5):694–704. [https://doi.org/10.1016/S1470-2045\(18\)30148-7](https://doi.org/10.1016/S1470-2045(18)30148-7).
- Foltz JA, Hess BT, Bachanova V, et al. Phase I trial of N-803, an IL15 receptor agonist, with Rituximab in patients with indolent Non-hodgkin Lymphoma. *Clin Cancer Res*. 2021;27(12):3339–50. <https://doi.org/10.1158/1078-0432.CCR-20-4575>.
- Karim C, Chang Sam S, Eugene K, et al. IL-15 superagonist NAI in BCG-Unresponsive non-muscle-invasive bladder Cancer. *NEJM Evid*. 2022;2(1):EVI-Doa2200167. <https://doi.org/10.1056/EVIDo2200167>.
- Sarhan D, Hippen KL, Lemire A, et al. Adaptive NK cells resist Regulatory T-cell suppression driven by IL37. *Cancer Immunol Res*. 2018;6(7):766–75. <https://doi.org/10.1158/2326-6066.CIR-17-0498>.
- Rowshanravan B, Halliday N, Sansom DM. CTLA-4: a moving target in immunotherapy. *Blood*. 2018;131(1):58–67. <https://doi.org/10.1182/blood-2017-06-741033>.
- Glasner A, Pliatas G. Tumor resident regulatory T cells. *Immuno-Oncol Focus Issue*. 2021;52:101476. <https://doi.org/10.1016/j.smim.2021.101476>.
- Simpson TR, Li F, Montalvo-Ortiz W, et al. Fc-dependent depletion of tumor-infiltrating regulatory T cells co-defines the efficacy of anti-CTLA-4 therapy against melanoma. *J Exp Med*. 2013;210(9):1695–710. <https://doi.org/10.1084/jem.20130579>.
- Ruchalski K, Braschi-Amirfarzan M, Douek M, et al. A primer on RECIST 1.1 for oncologic imaging in clinical drug trials. *Radiol Imaging Cancer*. 2021;3(3):e210008. <https://doi.org/10.1148/rycan.2021.210008>.
- Abel AM, Yang C, Thakar MS, Malarkannan S. Natural killer cells: Development, Maturation, and clinical utilization. *Front Immunol*. 2018;9. <https://doi.org/10.3389/fimmu.2018.01869>. <https://www.frontiersin.org/journals/immunology/articles/>.
- Cichocki F, Grzywacz B, Miller JS. Human NK Cell Development: One Road or Many? *Front Immunol*. 2019;10. <https://www.frontiersin.org/journals/immunology/articles/10.3389/fimmu.2019.02078>
- Stoeckius M, Hafemeister C, Stephenson W, et al. Simultaneous epitope and transcriptome measurement in single cells. *Nat Methods*. 2017;14(9):865–8. <https://doi.org/10.1038/nmeth.4380>.
- Yang C, Siebert JR, Burns R, et al. Heterogeneity of human bone marrow and blood natural killer cells defined by single-cell transcriptome. *Nat Commun*. 2019;10(1):3931. <https://doi.org/10.1038/s41467-019-11947-7>.
- Rubin CI, Atweh GF. The role of statmin in the regulation of the cell cycle. *J Cell Biochem*. 2004;93(2):242–50. <https://doi.org/10.1002/jcb.20187>.
- Jiang Y, Li Y, Zhu B. T-cell exhaustion in the tumor microenvironment. *Cell Death Dis*. 2015;6(6):e1792–1792. <https://doi.org/10.1038/cddis.2015.162>.

32. Makita S, Takatori H, Nakajima H. Post-transcriptional regulation of Immune responses and inflammatory diseases by RNA-Binding ZFP36 family proteins. *Front Immunol.* 2021;12. <https://doi.org/10.3389/fimmu.2021.711633>. <https://www.frontiersin.org/journals/immunology/articles/>.
33. Kim DO, Byun JE, Kim WS, et al. TXNIP regulates natural killer cell-mediated innate immunity by inhibiting IFN- γ production during bacterial infection. *Int J Mol Sci.* 2020;21(24). <https://doi.org/10.3390/ijms21249499>.
34. Crinier A, Dumas PY, Escalière B, et al. Single-cell profiling reveals the trajectories of natural killer cell differentiation in bone marrow and a stress signature induced by acute myeloid leukemia. *Cell Mol Immunol.* 2021;18(5):1290–304. <https://doi.org/10.1038/s41423-020-00574-8>.
35. Dean I, Lee CYC, Tuong ZK, et al. Rapid functional impairment of natural killer cells following tumor entry limits anti-tumor immunity. *Nat Commun.* 2024;15(1):683. <https://doi.org/10.1038/s41467-024-44789-z>.
36. Anthony SM, Rivas SC, Colpitts SL, Howard ME, Stonier SW, Schluns KS. Inflammatory signals regulate IL-15 in response to Lymphodepletion. *J Immunol.* 2016;196(11):4544–52. <https://doi.org/10.4049/jimmunol.1600219>.
37. Daniels MA, Luera D, Teixeira E. NF κ B signaling in T cell memory. *Front Immunol.* 2023;14. <https://www.frontiersin.org/journals/immunology/articles/10.3389/fimmu.2023.1129191>
38. Jin S, Guerrero-Juarez CF, Zhang L, et al. Inference and analysis of cell-cell communication using CellChat. *Nat Commun.* 2021;12(1):1088. <https://doi.org/10.1038/s41467-021-21246-9>.
39. Sharma A, Subudhi SK, Blando J, et al. Anti-CTLA-4 Immunotherapy does not deplete FOXP3 + Regulatory T cells (Tregs) in human cancers. *Clin Cancer Res.* 2019;25(4):1233–8. <https://doi.org/10.1158/1078-0432.CCR-18-0762>.
40. Berrien-Elliott MM, Becker-Hapak M, Cashen AF, et al. Systemic IL-15 promotes allogeneic cell rejection in patients treated with natural killer cell adoptive therapy. *Blood.* 2022;139(8):1177–83. <https://doi.org/10.1182/blood.2021011532>.
41. Bartel Y, Bauer B, Steinle A. Modulation of NK cell function by genetically coupled C-Type Lectin-Like Receptor/Ligand pairs encoded in the Human Natural Killer Gene Complex. *Front Immunol.* 2013;4. <https://doi.org/10.3389/fimmu.2013.00362>. <https://www.frontiersin.org/journals/immunology/article/>.
42. Zheng GXY, Terry JM, Belgrader P, et al. Massively parallel digital transcriptional profiling of single cells. *Nat Commun.* 2017;8(1):14049. <https://doi.org/10.1038/ncomms14049>.
43. Hao Y, Stuart T, Kowalski MH, et al. Dictionary learning for integrative, multi-modal and scalable single-cell analysis. *Nat Biotechnol.* 2024;42(2):293–304. <https://doi.org/10.1038/s41587-023-01767-y>.
44. Maynard KR, Collado-Torres L, Weber LM, et al. Transcriptome-scale spatial gene expression in the human dorsolateral prefrontal cortex. *Nat Neurosci.* 2021;24(3):425–36. <https://doi.org/10.1038/s41593-020-00787-0>.
45. Hao Y, Hao S, Andersen-Nissen E, et al. Integrated analysis of multimodal single-cell data. *Cell.* 2021;184(13):3573–e358729. <https://doi.org/10.1016/j.cell.2021.04.048>.
46. Hu C, Li T, Xu Y, et al. CellMarker 2.0: an updated database of manually curated cell markers in human/mouse and web tools based on scRNA-seq data. *Nucleic Acids Res.* 2023;51(D1):D870–6. <https://doi.org/10.1093/nar/gkac947>.
47. Aibar S, González-Blas CB, Moerman T, et al. SCENIC: single-cell regulatory network inference and clustering. *Nat Methods.* 2017;14(11):1083–6. <https://doi.org/10.1038/nmeth.4463>.
48. Love MI, Huber W, Anders S. Moderated estimation of Fold change and dispersion for RNA-seq data with DESeq2. *Genome Biol.* 2014;15(12):550. <https://doi.org/10.1186/s13059-014-0550-8>.
49. Qiu X, Mao Q, Tang Y, et al. Reversed graph embedding resolves complex single-cell trajectories. *Nat Methods.* 2017;14(10):979–82. <https://doi.org/10.1038/nmeth.4402>.
50. Liberzon A, Birger C, Thorvaldsdóttir H, Ghandi M, Mesirov JP, Tamayo P. The Molecular signatures Database Hallmark Gene Set Collection. *Cell Syst.* 2015;1(6):417–25. <https://doi.org/10.1016/j.cels.2015.12.004>.
51. Xu S, Hu E, Cai Y, et al. Using clusterProfiler to characterize multiomics data. *Nat Protoc.* 2024;19(11):3292–320. <https://doi.org/10.1038/s41596-024-01020-z>.

Publisher's note

Springer Nature remains neutral with regard to jurisdictional claims in published maps and institutional affiliations.